Crystallization study of model tetrahedral semiconductors

2002 J. Phys.: Condens. Matter 14 6627

(http://iopscience.iop.org/0953-8984/14/26/303)

INSTITUTE OF PHYSICS PUBLISHING JOURNAL OF PHYSICS: CONDENSED MATTER

J. Phys.: Condens. Matter **14** (2002) 6627–6638 PII: S0953-8984(02)35336-0

Crystallization study of model tetrahedral semiconductors

S M Nakhmanson[1,2] **and N Mousseau**[1,3]

[1] Department of Physics and Astronomy, Condensed Matter and Surface Science Program, Ohio University, Athens, OH 45701, USA
[2] Department of Physics, North Carolina State University, Raleigh, NC 27695, USA
[3] Département de Physique et Groupe de Recherche en Science et Technologie des Couches Minces, Université de Montréal, CP 6128, Succ. Centre-Ville, Montréal (Québec), Canada H3C 3J7

E-mail: nakhmans@nemo.physics.ncsu.edu and Normand.Mousseau@UMontreal.ca

Received 2 April 2002, in final form 20 May 2002
Published 21 June 2002
Online at stacks.iop.org/JPhysCM/14/6627

Abstract

The microscopic mechanisms leading to crystallization are not yet fully understood. This is due, in part, to the lack of atomistic as well as interatomic interaction models for a wide range of materials that can lead to crystallization on a computer-simulation timescale, i.e. <100 ns. While the nucleation in close-packed systems has been extensively studied, there are almost no numerical results for covalent tetrahedral semiconductors. We present here the simulation results of crystallization from the liquid and amorphous states of a 1000-atom model of silicon, described with a modified Stillinger–Weber potential. With this potential, it is possible to crystallize the model in as little as a few nanoseconds, which opens a door to detailed studies of the nucleation processes in covalent systems. Using topological analysis, we also present a first characterization of the structural fluctuations of the nucleation centres in this system and give a rough estimate for the critical size of these centres.

(Some figures in this article are in colour only in the electronic version)

1. Introduction

The nature of crystallization on the atomic level is a topic of major fundamental and technological interest. This is particularly true for covalent materials such as tetrahedral semiconductors, which show great variation in structure and density between the liquid and solid phases. These properties create some considerable challenges for a detailed microscopic understanding of the crystallization process in such materials: while crystallization of simple liquids has been realized numerically a long time ago [1–3], relatively little progress has been accomplished for simulations of more complex materials.

There exists a considerable body of literature, essentially experimental and computational, on crystallization in covalent materials, mostly Si (see [4–11]). It is usually possible to extract certain relevant information, such as crystallization interface velocity, from the experiments, but these measurements typically take place on a timescale too short for a detailed characterization of the onset of nucleation in these systems [6, 11]. In the area of computer simulations, the main efforts have been concentrated on the growth processes at crystal–liquid [4, 5] or amorphous–liquid [8] interfaces, which are important for understanding a number of experiments, including excimer laser crystallization and solid-phase epitaxial growth. Although providing important information about the structure of the liquid near the growth interface or the front velocity and the stability of different surface orientations, these simulations do not identify the basic mechanisms and topological structures responsible for nucleation. Studies addressing these particular issues in tetrahedral covalent materials are rare. Uttormark *et al* [7] provided a study of the crystal dissolution in liquid Si which seems to contradict the experimental conclusions of Stolk *et al* [6]. More recently, Bording and Taftø used the Tersoff's potential [12] to evaluate the relative stability of a crystalline grain in an amorphous matrix and identify the critical nucleus size for Ge [10]. However, in the aforementioned works a crystalline seed has to be placed into the system 'by hand', which produces an initial structure which might not be favoured by the dynamics of nucleation, as was shown recently for other materials [13].

The difficulty in reaching the same type of understanding for the nucleation of covalent solids as we have for Lennard-Jones systems is a problem of timescale. While the latter crystallize from the liquid in a matter of picoseconds, the time required for crystallization from the melt of Si or Ge is expected to be well beyond the reach of *ab initio* or tight-binding molecular dynamics. Empirical potentials, on the other hand, have numerous shortcomings [14] and have failed to reproduce the crystallization of covalent tetrahedral materials from the liquid phase.

In this paper, we revisit this problem using the modified Stillinger–Weber (mSW) interaction [15], a potential adjusted to generate a good quality amorphous phase for Si, i.e. with narrow spread of bond-angle distribution, very few coordination defects, and correct vibrational properties. Using this potential, we find that it is possible to crystallize both a liquid, from high temperature, and an amorphous network, heated from 0 K, providing a detailed microscopic picture of the process of crystallization. The grain growth, up to the limits of a 1000-atom cell, is almost isotropic and proceeds as soon as random fluctuations produce a crystalline cluster, containing $\approx$350–400 atoms. Because the mSW potential was not explicitly fitted to the liquid and crystalline phases of Si, our simulations are unlikely to describe any specific material in great detail; they should, however, provide a qualitative picture of crystallization in covalent materials, on a timescale reachable by the method of molecular dynamics.

The next section describes the details of our simulation techniques and our choice of order parameter used to monitor the level of crystallinity in a model. We then present the results for crystallization of our model from the liquid phase and from a molten amorphous configuration. For comparison, we also provide the results of the same simulation using the environment-dependent interaction potential (EDIP) of Justo *et al* [16], which shows how sensitive the timescale of crystallization is to the choice of potential. The explicit forms of the mSW potential and EDIP are given in the appendix.

2. Simulation details

We consider two routes to crystallization:

(1) starting from a liquid, we slowly cool the configuration below the melting point, until the diffusion becomes negligible; and

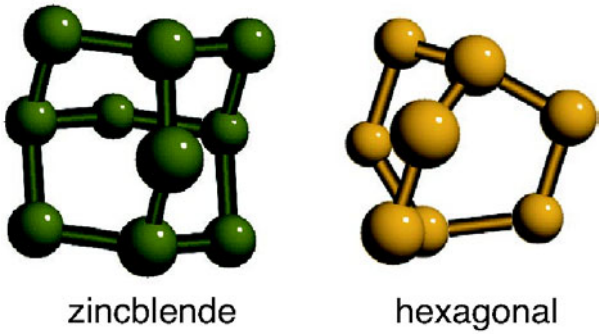

Figure 1. The two ring structures used as order parameters to characterize the state of crystallization in our simulation. Left, a ten-atom cluster with four sixfold rings forming the smallest topologically crystalline state in the zinc-blende structure. Right, an eight-atom cluster with three sixfold-membered rings back to back forming the smallest three-dimensional loop structure in hexagonal crystals.

(2) we heat a model of a-Si to a high temperature slightly below the melting point of the crystal and follow the recrystallization.

All the simulations are done with a 1000-atom cell, in the canonical ensemble, using Gauss's principle of least constraint to keep the temperature constant [17]. The density of the model in both cases is fixed to that of crystalline silicon.

There is some freedom in selecting an order parameter to follow the onset of crystallization. In Lennard-Jones systems, for example, researchers have used both cluster-based analysis [18, 19] and geometrical analysis based on icosahedral symmetries [20, 21]. Because of the covalent nature of the bonding in the mSW model, the cluster-based analysis is preferable in our case as it allows us to follow the crystallization process on a local scale. As both a-Si and c-Si show tetrahedral order, it is necessary to select clusters that contain more than just the first shell of neighbours. They are also required to be somewhat rigid, so that a topological analysis is sufficient to uniquely define the shape of these clusters. The two smallest topologically crystalline states in Si are three-dimensional ring structures, which can be employed as elementary building blocks of the zinc-blende (diamond-like) and hexagonal (ice-like) structures, as shown in figure 1. The first state is formed from four native sixfold rings, connected at alternating points along the rings. This 10-atom cage structure uniquely defines the basic building block of the zinc-blende structure. Although the hexagonal structure is not a ground state of silicon, it can also be encountered in small crystalline grains. We define the hexagonal building block as three sixfold rings, that are bonded together at two points forming an eight-atom structure. The density of these basic building blocks is close to zero in good quality a-Si models [22]. They represent, therefore, an excellent choice of order parameters for crystallization study.

To study crystallization from the liquid phase we employ the 'quench-from-the-melt' (QFM) technique which has already been used a number of times, with a wide variety of interactions [16, 23–25], to generate models of a-Si and a-Ge. In many previous simulations, during the cooling, the three-body interaction was often increased by 50–100% above the original SW values [23, 24, 26] in order to force the solidification of the model. No crystallization was reported in this early literature because the time system spent in the temperature range that favours this process was too short (tens of picoseconds instead of nanoseconds). As we show in the next section, even at this 'right' temperature—which is just below melting—the crystallization in our model does not start until at least after 0.5 ns.

Following the path of many previous simulations, we keep the volume fixed at the value corresponding to the experimental density of c-Si. Although such a procedure is hard to replicate experimentally, it simplifies the handling of thermodynamics around the phase transition and makes it easier to compare with other simulations. Given the difficulty previously encountered in crystallizing a complex liquid, a constant-volume simulation should minimize the number of hurdles slowing down the crystallization process. Such constraint is not formally necessary, however, and constant-pressure simulations are under way.

3. Results

3.1. Crystallization from the liquid phase

Our simulation proceeds as follows:

(i) The 1000-atom c-Si supercell is melted during a 2 ns constant-temperature anneal at 3000 K, well above the c-Si melting point for mSW potential.
(ii) The supercell is then gradually cooled down by reducing the temperature in 200 K steps in the 3000–2400 K interval and 100 K steps below 2400 K, and running for 0.5 ns at each step.

The simulation is stopped when diffusion becomes negligible. The results for this simulation are summarized in figures 2 and 3. At 3000 K, the radial distribution function, $g(R)$, of our model exhibits liquid-like behaviour, showing features similar to those computed for l-Si by Cook and Clancy [14] using Tersoff's potential [12]; this is confirmed by the atomic diffusion shown in figure 3. As with Tersoff's potential, the structure in the $g(R)$ beyond the first-neighbour peak at high temperature is likely due to a low atomic density and a relatively strong three-body interaction.

As the annealing temperature goes down (2400–2100 K), the $g(R)$ becomes more structured and starts resembling that of a-Si: the dip between the first- and second-neighbour peaks deepens and the peaks narrow. Below 2100 K, however, the broad second-neighbour peak begins to split into two narrower peaks corresponding to atomic shells in the *crystalline* structure. Other peaks also start forming beyond 5 Å. The crystallization process can also be followed with atomic diffusion (figure 3), which decreases smoothly in the liquid phase but falls brutally as the temperature of the system is brought from 2100 to 1900 K, when the lattice essentially freezes over.

The structural data for the model, after quenching to 0 K, for final annealing temperatures of 2100, 2000, and 1900 K is shown in figure 4. There is a clear qualitative structural change among these three structures. The structure annealed at 2100 K shows properties typical of a very good amorphous model: the dihedral-angle distribution is structureless, the bond-angle distribution is almost a Gaussian of width 11.16° and the $g(R)$ is smooth with a clear gap between the first- and second-neighbour shells. This is in sharp contrast with the structures at 2000 and 1900 K where the bond-angle distributions have widths of 8.57 and 6.41°, the dihedral-angle distributions develop a sharp peak at 60° and the $g(R)$ is clearly crystalline.

The role of the potential in achieving crystallization is underscored by a simulation, performed in the same fashion but with EDIP [16]. Starting from the liquid phase at 2300 K, as prepared using mSW, the cell is re-equilibrated with EDIP at the same temperature for 0.5 ns. The temperature is then lowered in 100 K steps, running for 0.5 ns at each temperature, until the diffusion becomes negligible. As shown in figure 5, the supercooled regime persists to a much lower temperature than in the case of the mSW anneal. The atomic diffusion (not shown) stops only at around 1100 K, at which point, the structure freezes in a good

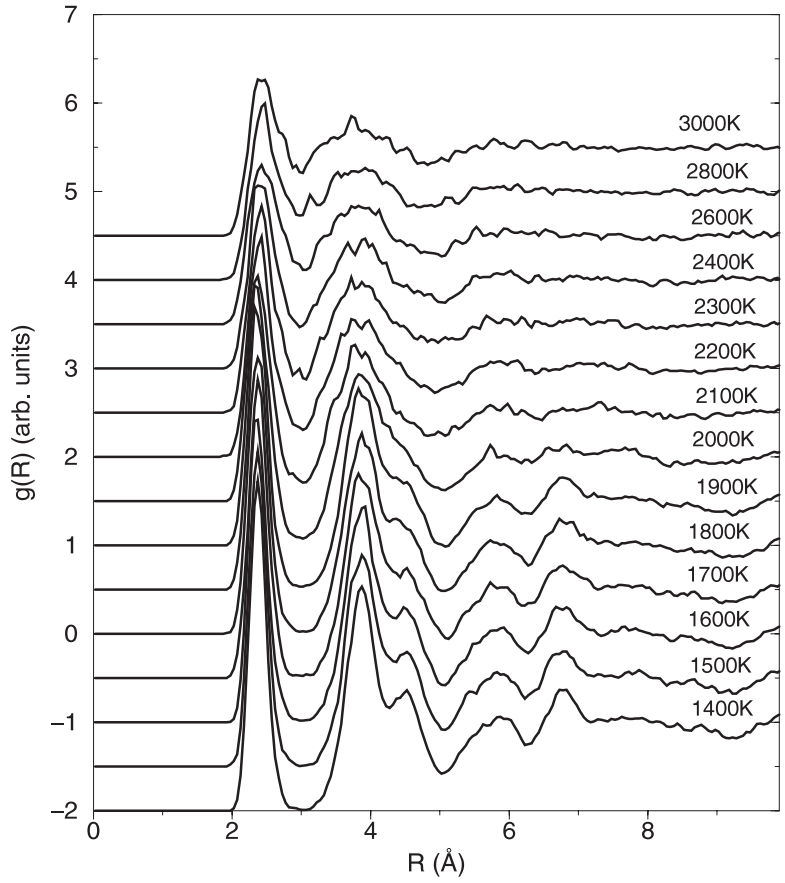

Figure 2. The radial distribution function, $g(R)$, for the 1000-atom QFM model, created with the mSW potential, calculated after anneals (with no subsequent quench) at different annealing temperatures.

quality amorphous configuration. There is no hint of crystallization at any point during the simulation. The difference in system's behaviour upon cooling with the mSW potential or EDIP can be attributed to the fact that in the liquid phase the former potential favours the fourfold environment, which helps to achieve crystallization after a few nanoseconds.

3.2. Crystallization from the amorphous phase

In order to better characterize the crystallization process, we also perform a constant-temperature anneal for the 1000-atom model of Barkema and Mousseau [27] prepared using a bond-switching method. Prior to the main simulation, we have computed the atomic diffusion in the model at several constant temperatures and found that for the mSW potential it becomes substantial (larger than the atomic bond length per nanosecond) above $T \approx 2000$ K. The main simulation is then done at 2100 K, for 2 ns, with atomic coordinates saved every 200 fs. Figure 6 shows the two order parameters, i.e. the number of cubic and hexagonal building blocks, as a function of time for this simulation. At the beginning of the simulation, the cell is mostly disordered, with very little crystalline structure; between 0.6 and 0.9 ns, however, we see a rapid ordering, with more than 98% of the atoms belonging to crystalline building blocks

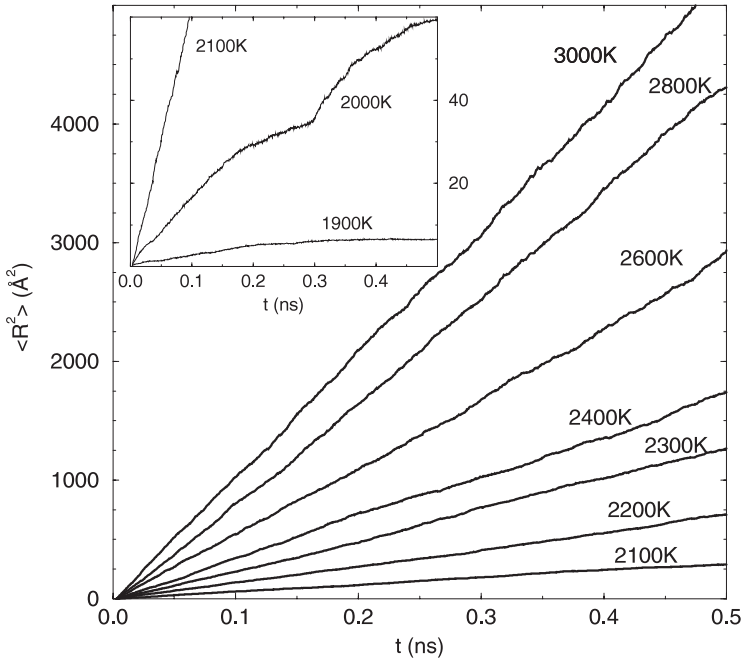

Figure 3. Diffusion in the 1000-atom QFM model for Si, created with the mSW potential, during anneals in 3000–2100 and 2100–1900 K (see inset) temperature intervals.

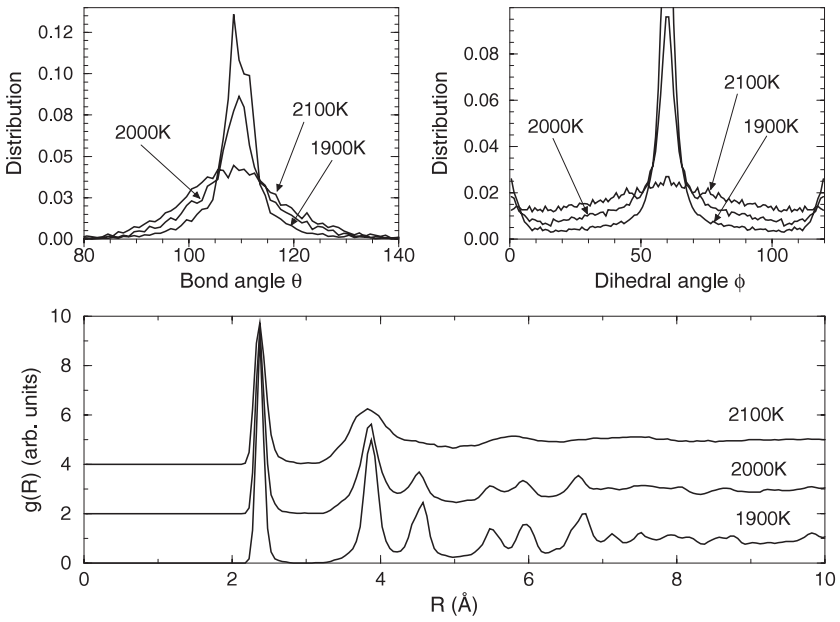

Figure 4. Bond-angle (upper left panel) and dihedral-angle (upper right panel) distributions, and the $g(R)$ for 1000-atom QFM model for Si, created with the mSW potential, calculated after annealing and subsequent quenching for annealing temperatures of 2100, 2000, and 1900 K.

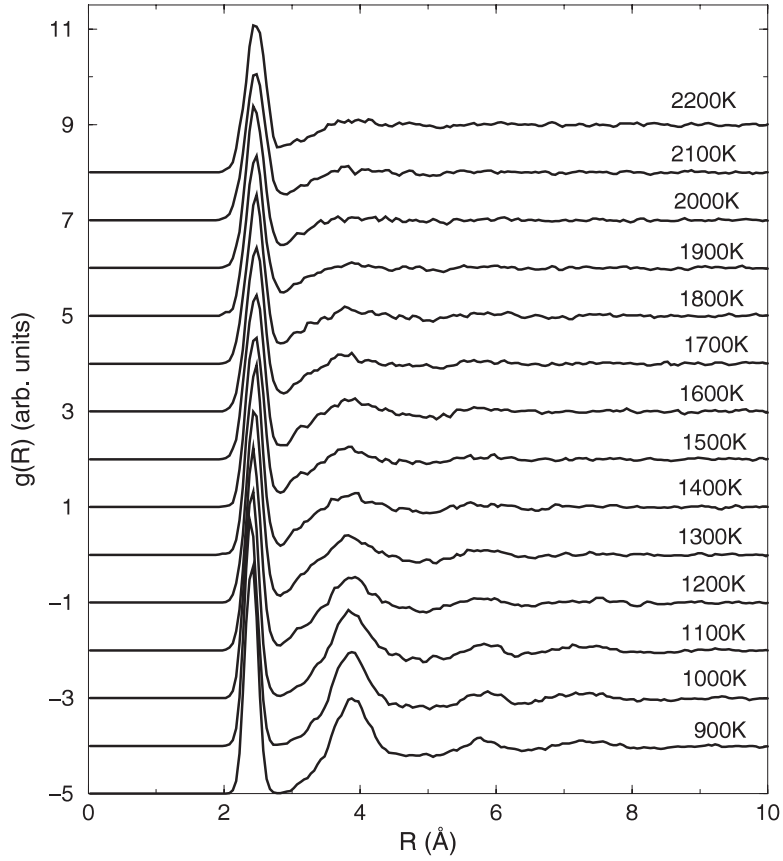

Figure 5. The $g(R)$ for the 1000-atom QFM model for Si, created with EDIP, calculated after anneals (with no subsequent quench) at different annealing temperatures.

at the end of this time interval. The second nanosecond shows only local rearrangements, but no overall rebonding. This transition can also be followed in the diffusion data, shown in the right inset of figure 6. In the early time of the simulation, the amorphous solid essentially melts, with a total diffusion of about 10 Å/atom, but as soon as crystallization has taken place the diffusion slows down to almost zero. This agrees with a well known fact that experimental melting point of a-Si is lower than that of its crystalline counterpart [28]. In the left inset of the same figure we show the number of atoms belonging to the crystalline island (the largest cluster constructed of *interconnected* crystalline building blocks) as the simulation goes on. We can see that the process of crystallization starts when the island contains 350–400 atoms. We should point out, however, that our choice of elementary building blocks tends to *overestimate* the size of crystalline islands because, first, even substantially strained network regions are considered crystalline if they retain crystalline bonding and, second, the building blocks include many atoms, some of which could be only marginally crystalline. For example, the number of clusters in the crystal nucleus is about 300, out of a total of 3000 for this 1000-atom model, i.e., only 10% of all clusters are formed at this point. Using a similar atomic proportion would give a critical size of about 100 atoms. This number is in line with a critical nucleus of about 200 atoms found for stabilizing a crystallite of Si in an amorphous matrix, as reported in a numerical study by Bording and Taftø [10].

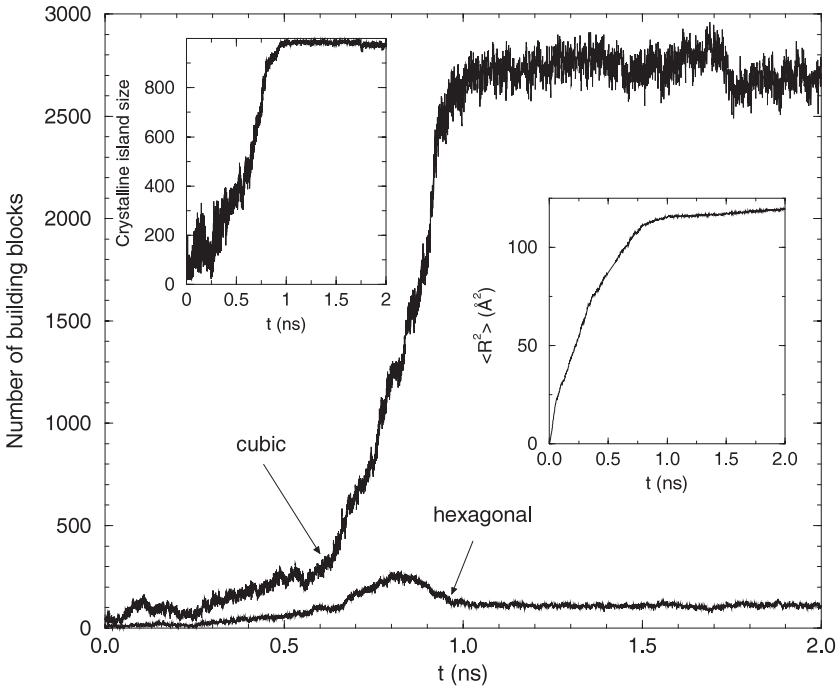

Figure 6. The number of cubic and hexagonal building blocks in 1000-atom model of a-Si during a 2 ns constant-temperature anneal with the mSW potential. The atomic diffusion and the number of atoms in a crystalline island are shown on the insets.

With the help of figure 7, the simulation gives us some insight into the crystallization process in covalent materials. Although the potential only goes out to second neighbours, even in the initial stage of the simulation (the first 0.5 ns) small 'crystallites', that are constantly formed and destroyed, are mostly composed of the cubic blocks (see, for example, figures 7(a) and (b)). Around 0.5 ns, a larger crystalline island emerges (see figure 7(c)) and starts growing rapidly. New crystallites, mainly of hexagonal type, are formed at the surface of the island. It soon reaches the size of the unit cell and forms grain boundaries between itself and its images, as shown in figures 7(d) and (e). Again, these grain boundaries contain mainly hexagonal blocks, while the core of the island consists of cubic blocks. At 0.9 ns almost all of the supercell has become crystalline (figure 7(f)) and only a few thin hexagonal-type grain-boundary sheets are left in the system. It is worth noting that the position of the peak in hexagonal-block concentration at 0.6–0.8 ns in figure 6 coincides well with the kink in the cubic-block concentration marking the disordered-to-crystalline transition which is due to the fact that, according to the data presented in figure 7, the island growth during the transition proceeds mainly by forming new hexagonal blocks on the island's surface.

These figures do not indicate any preferential orientation for the growth of the nucleus, in agreement with the work of Bording and Taftø [10] on the growth of a crystal seed in an amorphous matrix but in contrast with the results of the pioneering work of Landman and Luedtke [5] on epitaxial crystal growth from the melt. This might be due to the fact that both the Bording–Taftø and our simulations were done at constant temperature, while that of Landman and Luedtke simulated the propagation of a laser pulse, therefore imposing a heat flow.

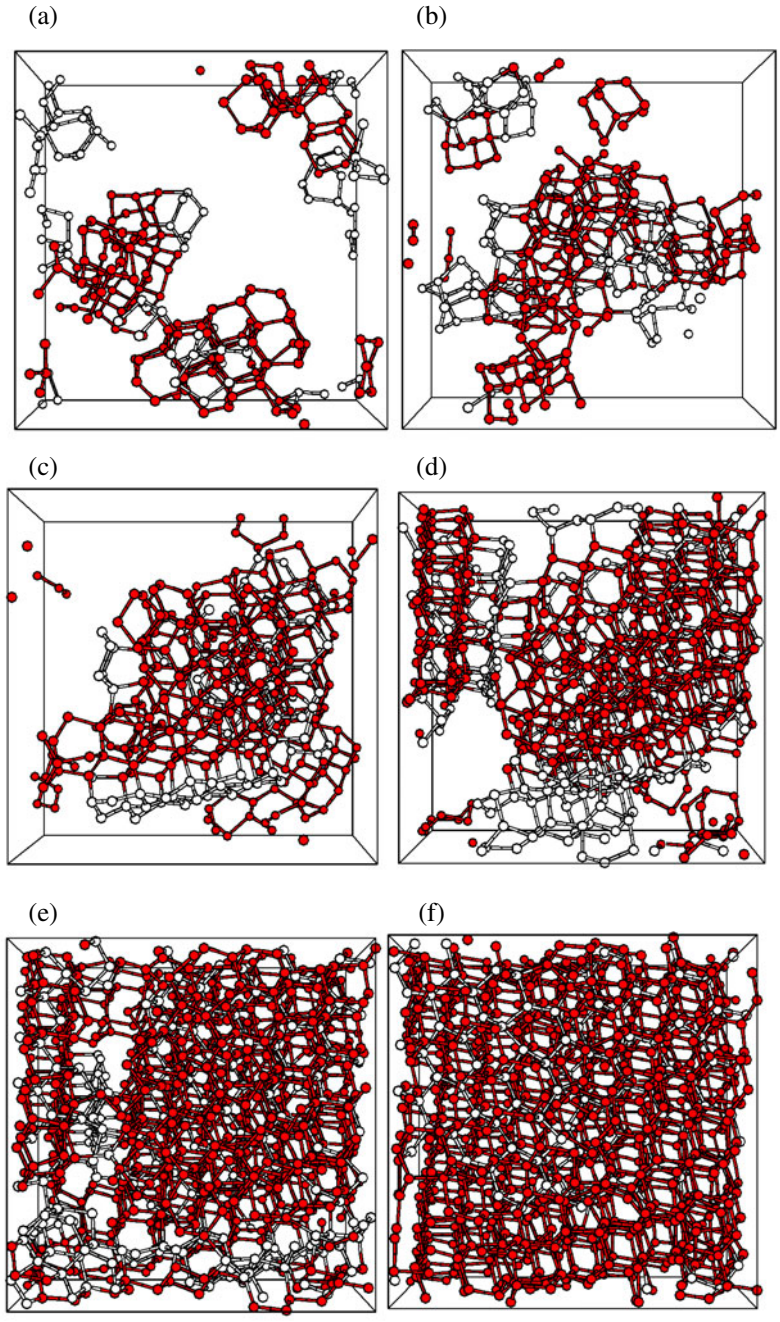

Figure 7. Crystalline islands in the 1000-atom model of a-Si during a 2 ns constant-temperature anneal with the mSW potential: (a) at 100 ps, (b) at 300 ps, (c) at 500 ps, (d) at 700 ps, (e) at 800 ps, and (f) at 1 ns. Atoms shown in dark grey and white belong to cubic and hexagonal blocks respectively. Atoms not belonging to any crystalline building blocks are not shown.

4. Conclusions

The last few years have seen a resurgence of interest in the onset of crystallization. While numerical studies have been mostly limited to close-packed materials, we have shown that it is now possible to also study this phenomenon in tetrahedral covalent semiconductors. We found that, during the growth, the interface with the liquid contains a high density of hexagonal building blocks that transform into zinc-blende-type blocks as the crystal grows. This phenomenon has not been reported in any other experiment or simulation of crystal growth and will be studied in details in future. Obviously, much more work is required to gain understanding of the nucleation process in tetrahedral covalent materials on the level of quantitative predictions (nucleation and growth rate, defect density, etc). More realistic simulations for larger models are under way to characterize the phase diagram of the system and the details of the nucleation process in it.

Acknowledgments

This work was supported in part by NSF under grants number DMR 00-81006 and DMR 98-05848 as well as NSERC (Canada) and NATEQ (Quebec). We thank G T Barkema for providing us with the crystalline cluster analysis code for Si. NM is a Cottrell Scholar from the Research Corporation.

Appendix

Both the Stillinger–Weber potential [15] and the environment-dependent interatomic potential of Justo *et al* [16] for silicon can be described with a general formula, containing two- and three-body interatomic interactions:

$$E(\{\boldsymbol{R}_i\}) = \sum_{\langle i,j\rangle} v_2(R_{ij}, Z_i) + \sum_{\langle i,j,k\rangle} v_3(\boldsymbol{R}_{ij}, \boldsymbol{R}_{ik}, Z_i), \tag{A.1}$$

where $\{\boldsymbol{R}_i\}$ is the set of atomic coordinates and Z_i is a local-environment parameter for atom i.

For the Stillinger–Weber potential, which does not explicitly depend on the parameter Z_i, the two- and three-body interaction terms have the following form:

$$v_2(R_{ij}) = \epsilon A\left[B\left(\frac{R_{ij}}{\sigma}\right)^{-p} - 1\right]\exp\left\{\frac{1}{R_{ij}/\sigma - a}\right\}\Theta(R_{ij}/\sigma - a), \tag{A.2}$$

$$v_3(\boldsymbol{R}_{ij}, \boldsymbol{R}_{ik}) = \epsilon\lambda\exp\left[\frac{\gamma}{R_{ij}/\sigma - a} + \frac{\gamma}{R_{ik}/\sigma - a}\right] \times (\cos\theta_{jik} + 1/3)\Theta(R_{ij}/\sigma - a)\Theta(R_{ik}/\sigma - a). \tag{A.3}$$

Here $\Theta(x)$ is the Heaviside step function, θ_{jik} is the angle between bonds R_{ij} and R_{ik}, and ϵ, A, B, σ, p, a, λ, and γ are the fitting parameters (see table A.1). The interaction range of the potential is governed by parameters σ and a, that place the interaction cut-off at $\approx$3.77 Å—between the first-and second-neighbour distances for c-Si. The main property of the three-body term is that it penalizes any deviation from an ideal diamond structure bond angle (for which $\cos\theta_{jik} = -1/3$), thus favouring perfect tetrahedral bonding in the material.

In EDIP, on the other hand, both interaction terms carry an explicit dependence on local-environment parameter $Z_i = \sum_{m\neq i} f(R_{im})$, where $f(R_{im})$ is a cut-off function that measures the contribution of neighbour m to the coordination of atom i in terms of interatomic separation R_{im}.

Table A.1. Parameters for the standard and mSW potentials.

Parameter	Standard SW	Modified SW
ϵ (eV)	2.168 26	1.648 33
A	7.049 556 277	7.049 556 277
B	0.602 224 5584	0.602 224 5584
σ (Å)	2.095 1	2.095 1
p	4	4
a	1.80	1.80
λ	21.0	31.5
γ	1.20	1.20

The two-body term of the potential includes repulsive and attractive interactions:

$$v_2(R_{ij}, Z_i) = A\left[\left(\frac{B}{R_{ij}}\right)^{\rho} - p(Z_i)\right]\exp\left\{\frac{\sigma}{R_{ij} - a}\right\}, \tag{A.4}$$

which go to zero at the cut-off distance a ($\approx$3.12 Å). The environment-dependent part is represented by a Gaussian function: $p(Z_i) = \exp(-\beta Z_i)$.

The three-body term contains radial and angular parts:

$$v_3(\boldsymbol{R}_{ij}, \boldsymbol{R}_{ik}, Z_i) = g(R_{ij})g(R_{ik})h(\cos\theta_{jik}, Z_i), \tag{A.5}$$

where the radial function $g(r) = \exp(\gamma/(r - a))$ has the same form as for the Stillinger–Weber potential and goes to zero smoothly at the cut-off distance a. The angular function $h(\cos\theta, Z)$ has strong dependence on the local coordination through two functions that control the equilibrium angle and the interaction strength. Its detailed description is provided in [29].

References

[1] Frenkel D and McTague J P 1980 *Annu. Rev. Phys. Chem.* **31** 491
[2] Oxtoby D W 1988 *Adv. Chem. Phys.* **70** 263
[3] Huitema H E A, van der Eerden J P, Janssen J J M and Human H 2000 *Phys. Rev.* B **62** 14 690
[4] Abraham F F and Broughton J Q 1986 *Phys. Rev. Lett.* **56** 734
[5] Landman U, Luedtke W D, Ribarsky M W, Barnett R N and Cleveland C L 1988 *Phys. Rev.* B **37** 4637
Luedtke W D, Landman U, Ribarsky M W, Barnett R N and Cleveland C L 1988 *Phys. Rev.* B **37** 4647
[6] Stolk P A, Polman A and Sinke W C 1993 *Phys. Rev.* B **47** 5
[7] Uttormark M J, Thompson M O and Clancy P 1993 *Phys. Rev.* B **47** 15 717
[8] Brambilla L, Colombo L, Rosato V and Cleri F 2000 *Appl. Phys. Lett.* **77** 2337
[9] Lee M, Moon S, Hatano M, Suzuki K and Grigoropoulos C P 2000 *J. Appl. Phys.* **88** 4994
[10] Bording J K and Taftø J 2000 *Phys. Rev.* B **62** 8098
[11] Hatano M, Moon S, Lee M, Suzuki K and Grigoropoulos C P 2000 *J. Appl. Phys.* **87** 36
[12] Tersoff J 1986 *Phys. Rev. Lett.* **56** 632
Tersoff J 1988 *Phys. Rev.* B **37** 6991
Tersoff J 1988 *Phys. Rev.* B **38** 9902
[13] Yau S-T and Vekilov P G 2000 *Nature* **406** 494
Seeley L H and Seidler G T 2001 *Phys. Rev. Lett.* **87** 055702
[14] Cook S J and Clancy P 1993 *Phys. Rev.* B **47** 7686
[15] Stillinger F H and Weber T A 1985 *Phys. Rev.* B **31** 5262
Vink R L C, Barkema G T, van der Weg W F and Mousseau N 2001 *J. Non-Cryst. Solids* **282** 248
[16] Justo J F, Bazant M Z, Kaxiras E, Bulatov V V and Yip S 1998 *Phys. Rev.* B **58** 2539
[17] Evans D J, Hoover W G, Failor B H, Moran B and Ladd A J C 1983 *Phys. Rev.* A **28** 1016
Gauss K F 1829 *J. R. Angew. Math.* **4** 232
[18] Honeycutt J D and Andersen H C 1987 *J. Chem. Phys.* **91** 4950
[19] Báez L A and Clancy P 1995 *J. Chem. Phys.* **102** 8138
[20] Frank F C 1952 *Proc. R. Soc.* A **215** 43

[21] Steinhardt P J, Nelson D R and Ronchetti M 1983 *Phys. Rev.* B **28** 784
[22] Barkema G T and Mousseau N, unpublished
[23] Ding K and Andersen H C 1986 *Phys. Rev.* B **34** 6987
[24] Luedtke W D and Landman U 1988 *Phys. Rev.* B **37** 4656
[25] Kim E and Lee Y H 1994 *Phys. Rev.* B **49** 1743
Car R and Parrinello M 1988 *Phys. Rev. Lett.* **60** 204
[26] Broughton J Q and Li X P 1987 *Phys. Rev.* B **35** 9120
[27] Barkema G T and Mousseau N 2000 *Phys. Rev.* B **62** 4985
[28] Donovan E P, Spaepen F, Turnbull D, Poate J M and Jacobson D C 1983 *Appl. Phys. Lett.* **42** 698
[29] Bazant M Z, Kaxiras E and Justo J F 1997 *Phys. Rev.* B **56** 8542